

ContraGS: Codebook-Condensed and Trainable Gaussian Splatting for Fast, Memory-Efficient Reconstruction

Sankeerth Durvasula^{1†}, Sharanshagar Muhunthan¹, Zain Moustafa¹, Richard Chen¹, Ruofan Liang¹
Yushi Guan¹, Nilesh Ahuja², Nilesh Jain², Selvakumar Panneer², Nandita Vijaykumar¹

¹University of Toronto ²Intel

{sankeerth, zain, ruofan, guanyushi, nandita}@cs.toronto.edu

{shangar.muhunthan, riixardo.chen}@mail.utoronto.ca

{nilesh.ahuja, nilesh.jain, selvakumar.panneer}@intel.com

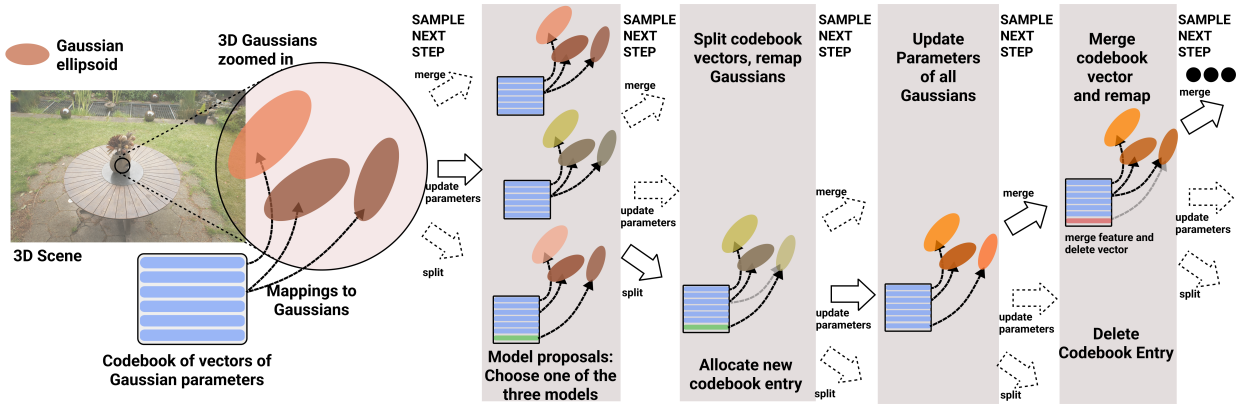


Figure 1. ContraGS: A 3D scene is modeled using 3D Gaussian Splatting [25]. A codebook stores a compressed representation of the 3DGS scene as common vectors of 3DG parameters. ContraGS enables learning parameters of a codebook-compressed 3DG scene by posing the parameter estimation as a Bayesian inference problem. ContraGS proposes split/merge/update on each codebook vector to explore the state space of codebook-compressed models.

Abstract

3D Gaussian Splatting (3DGS) is a state-of-art technique to model real-world scenes with high quality and real-time rendering. Typically, a higher quality representation can be achieved by using a large number of 3D Gaussians. However, using large 3D Gaussian counts significantly increases the GPU device memory for storing model parameters. A large model thus requires powerful GPUs with high memory capacities for training and has slower training/rendering latencies due to the inefficiencies of memory access and data movement. In this work, we introduce ContraGS, a method to enable training directly on compressed 3DGS representations without reducing the Gaussian Counts, and thus with a little loss in model quality. ContraGS leverages codebooks to compactly store a set of Gaussian parameter vectors throughout the training process, thereby significantly reducing mem-

ory consumption. While codebooks have been demonstrated to be highly effective at compressing fully trained 3DGS models, directly training using codebook representations is an unsolved challenge. ContraGS solves the problem of learning non-differentiable parameters in codebook-compressed representations by posing parameter estimation as a Bayesian inference problem. To this end, ContraGS provides a framework that effectively uses MCMC sampling to sample over a posterior distribution of these compressed representations. With ContraGS, we demonstrate that ContraGS significantly reduces the peak memory during training (on average $3.49\times$) and accelerated training and rendering ($1.36\times$ and $1.88\times$ on average, respectively), while retraining close to state-of-art quality.

1. Introduction

3D Gaussian Splatting [25] (3DGS) is a state-of-art technique for modeling real-world scenes with high quality and

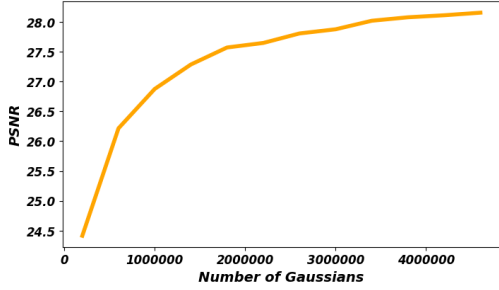


Figure 2. Impact of number of Gaussians on representation quality for the “Truck” scene of T&T [27], using 3DGS-MCMC [26]

real-time rendering. It is a powerful scene representation method applicable to various tasks, including 3D/4D reconstruction [13, 34, 40, 56, 64, 67, 68], simultaneous localization and mapping (SLAM) [21, 22, 60–62], 3D object generation [14, 23, 53, 71] 3D editing [3, 4, 45, 49, 57, 63, 65] simulation [1, 32, 58, 59], representing detailed human avatars [24, 28, 42, 43, 48, 51, 52, 66], etc. 3DGS represents scenes with a collection of 3D Gaussians associated with a view-dependent emitted radiance (color). The parameters defining the position, shape and color of each Gaussian are obtained by minimizing a photometric loss using gradient descent.

Learning very high quality scene representations with 3DGS, especially for complex scenes, typically requires a large number of 3D Gaussians. Fig. 2 shows the reconstruction quality (PSNR) vs. the number of Gaussians used to represent the “Truck” scene [27], using the state-of-art approach 3DGS-MCMC [26]. 2 million Gaussians achieves a PSNR of 27.64, whereas 4 million Gaussians achieves a PSNR of 28.15. Using more Gaussians, however, incurs much larger memory overheads during both training/inference and for storage. For example, representing the Truck scene [27] with Gaussians requires over 2 GB of memory for the model alone. Efficiently learning scenes with high Gaussian counts thus necessitates a powerful GPU with large memory capacity. The peak memory needed for training can be as much as $4\times$ the model size in order to save intermediate values during rendering and gradient computation. In addition to requiring GPUs with large memory capacities, this also significantly slows down the training process due to the large data movement overheads. Thus, training complex scenes with 3DGS is challenging on environments such as mobile devices, web browsers, and other resource-constrained platforms.

A range of recent works [10, 18, 31, 47, 55] propose post-training compression methods to reduce the amount of memory required to store a 3DGS model. However, these works still incur the full memory cost *during* training. Other prior works [15, 17, 36, 38] reduce model size during training by pruning redundant Gaussians. However, this results in lower quality models than those that can be achieved with

a larger number of Gaussians (Section 5.2).

In this work, we aim to enable high-speed memory-efficient training and rendering without sacrificing the quality of a 3DGS scene with high Gaussian counts. To this end, we leverage codebook representations [7, 10, 47] that can significantly reduce the memory required to store 3DGS parameters. Codebooks reduce the model’s memory footprint by storing a small set of vectors containing parameters shared among Gaussians, instead of storing an independent set of parameters for each Gaussian. Each Gaussian maps to one vector in the codebook. Codebooks have been demonstrated to be highly effective at compressing fully trained 3DGS models [7, 10, 47] as a *post-training* optimization. However, leveraging codebook compression *during training* is an unsolved challenge. The parameters in the codebook compressed representation are (a) the codebook vectors and (b) the mapping between Gaussians and their codebook vectors. These non-differentiable indexes that map Gaussians to codebook vectors cannot be learnt by SGD.

In this work, we solve the problem of directly learning on codebook-compressed representations by using MCMC sampling to sample over a posterior distribution of these compressed representations. Posing the parameter estimation as Bayesian inference over a posterior distribution [26], instead of an optimization problem, offers the opportunity to estimate the non-differentiable compressed-3DGS parameters. However, using Stochastic Gradient Langevin Dynamics (SGLD), a method for Bayesian inference as proposed by prior work, 3DGS-MCMC [26] will not work for codebook-compressed representations. This is because SGLD also requires the differentiability of the log-posterior distribution with respect to estimated parameters.

We propose ContraGS, a method for learning codebook-compressed representations via Bayesian inference. We use the Metropolis-Hastings algorithm, a Markov Chain Monte Carlo sampling method, to sample from the posterior distribution. An overview of ContraGS is shown in Fig. 1. Starting from an initialized set of mappings between the Gaussians and the codebook, ContraGS defines a proposal distribution that generates new candidate compressed 3DGS-models with a different set of Gaussian-to-Codebook mappings. This new set of models is obtained by either splitting/cloning a set of codebook vectors into two vectors or merging pairs of codebook vectors into one vector. Gaussians are remapped to the new codebook vectors generated by splitting/merging. Different sequences of splitting and merging operations will generate all possible codebook-compressed model representations. Some steps may simply update the values of the codebook vectors without affecting the mapping. Thus, proposals drawn from this distribution enable exploration of the complete state space of codebook-compressed models.

We demonstrate that ContraGS enables high-speed

memory-efficient training without sacrificing the model quality significantly. With 2 million Gaussians used to represent the scene, ContraGS reduces the peak model memory by $3.49\times$ on average during training. This accelerates training by $1.36\times$ on average and increases the final model’s rendering FPS by $1.88\times$ on average. Our contributions can be listed as follows:

- This is the first proposed method that enables 3DGS training directly on compressed representations.
- We propose a novel mathematical framework to jointly learn codebook vectors and their mappings to model parameters, achieving efficient compression *during* training. We formulate codebook compression as an MCMC sampling problem over a posterior distribution. We use this approach to learn non-differentiable codebook indices by exploring the state space of possible codebook mappings during MCMC sampling. This framework can be applied to learn other codebook-compressed point-based 3D reconstruction methods to enable fast, memory efficient training such as RadiantFoam [16], ADOP [50], Deformable Beta Splatting [35] and LinPrim [54].
- We show how adopting a Bayesian inference formulation over a posterior allows incentivising smaller codebooks sizes for higher compression.
- We demonstrate that ContraGS significantly reduces peak memory during training while retaining close to state-of-art quality. For any memory capacity constraint (i.e. peak memory utilization), ContraGS achieves the highest representation quality compared to prior works.

2. Background

2.1. 3DGS Scene Representation

Point-based scene representation techniques, such as 3DGS [25], represent 3D scenes with a collection of anisotropic 3D Gaussian densities in space. The i^{th} Gaussian distribution G_i is given by:

$$G_i(\mathbf{r}) = o_i \exp \left\{ -\frac{1}{2}(\mathbf{r} - \boldsymbol{\mu}_i)^T \Sigma_i^{-1}(\mathbf{r} - \boldsymbol{\mu}_i) \right\} \quad (1)$$

Where \mathbf{r} is a 3D position, o_i is the opacity, $\boldsymbol{\mu}_i$ is the location of its center, and Σ_i is the covariance. Σ_i is expressed as:

$$\Sigma = R(\mathbf{q})SS^TR(\mathbf{q})^T \quad (2)$$

Where $R(\mathbf{q})$ represents the rotation matrix described by the quaternion \mathbf{q} , and S is a diagonal matrix corresponding to principal axis scales. Rendering the scene for a camera pose \mathcal{P} involves determining the color \mathbf{C} of each pixel x , the scene comprising Gaussians can be rendered using the following equations:

$$\mathbf{C}(x) = \sum_{k=1}^N \alpha_k(x) c_k \prod_{i=1}^{k-1} (1 - \alpha_i(x)) \quad (3)$$

Here, α_i is the 2D Gaussian projected from the 3D Gaussian density (Eq. 1) onto the camera plane. c_i is the color of the 3D Gaussian as seen in the viewing direction.

From a set of M images $I_{\mathcal{P}_1}, I_{\mathcal{P}_2}, I_{\mathcal{P}_3}, \dots, I_{\mathcal{P}_M}$ of a 3D scene taken from viewing directions $\mathcal{P}_1, \mathcal{P}_2, \mathcal{P}_3, \dots, \mathcal{P}_M$, 3D reconstruction aims to determine the 3D Gaussians parameters that capture the 3D scene. Parameters are determined by minimizing a loss function $\mathcal{L}_{\text{recon}}$, which measures the accuracy of reconstruction. $\mathcal{L}_{\text{recon}}$ is expressed as:

$$\mathcal{L}_{\text{recon}} = (1 - \lambda_{\text{ssim}}) \mathcal{L}_1 + \lambda_{\text{ssim}} \mathcal{L}_{\text{SSIM}} \quad (4)$$

Here, \mathcal{L}_1 and $\mathcal{L}_{\text{SSIM}}$ are the averaged L1 and Structural Similarity (SSIM) losses between the rendered and ground-truth images. The parameters that minimize the loss function are determined using gradient descent.

2.2. Codebooks to Store 3DG Parameters

3D scenes typically consist of many Gaussians with similar sets of parameters. The memory needed for storing these redundant Gaussian parameters can be reduced by using codebooks. A codebook is a small set of vectors storing 3D Gaussian parameters. Each Gaussian is mapped to a vector in the codebook. A Gaussian’s parameters can be obtained by looking up the mapped vector in the codebook.

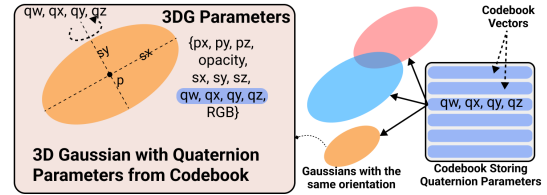


Figure 3. Gaussians mapped to one vector in a codebook of quaternions (right hand side). One Gaussian among them, whose quaternions are derived from the codebook vector is shown on the left.

C3DGS [47] uses codebooks to compress 3DGS scene. It uses one codebook to store spherical harmonics coefficients, and another codebook to store covariance parameters (rotation quaternion and principal axis scales) as shown in Fig. 3. Each Gaussian is mapped to one vector in the SH feature codebook, and one vector in the covariance codebook. Note that although we adopt a similar codebook indexing scheme as C3DGS [47], our method does not restrict us from choosing this specific way of choosing codebooks.

2.3. 3DGS Training as MCMC Sampling

3DGS-MCMC [26] demonstrated that the training process of 3DGS can be interpreted as performing bayesian inference over the probability distribution function given by:

$$p(G) = \frac{1}{Z} \exp(-\mathcal{L}_{\text{recon}}(G)) \quad (5)$$

Here, G is the set of parameters of all Gaussians in the scene, Z is a normalizing constant to the probability distribution. $\mathcal{L}_{\text{recon}}$ is the reconstruction loss given by Eq. 4,

written as a function over Gaussian parameter G . Bayesian inference is performed by sampling a set of Gaussian parameter values G_{recon} from the distribution p (denoted as $G_{\text{recon}} \sim p$). Sampling from this high dimensional distribution function can be performed using Markov Chain Monte Carlo (MCMC) sampling.

2.3.1. MCMC Sampling via Metropolis-Hastings

MCMC is used to sample from high dimensional probability distributions. Consider a high-dimensional state space X , and a probability distribution function p_X defined over it. Our goal is to generate samples x from this distribution, denoted as $x \sim p_X$. One such MCMC sampling algorithm is the Metropolis-Hastings (MH) [19]. MH is implemented by constructing two distributions:

- **Proposal distribution:** Denoted as $q(x_i \rightarrow x_j)$, the proposal distribution q specifies the probability of transitioning from each state in the state space x_i to state x_j .
- **Acceptance distribution:** Denoted as $A(x_i \rightarrow x_j)$, the acceptance distribution determines whether a proposed transition is accepted. Specifically, it is defined as:

$$A(x_i \rightarrow x_j) = \min \left(1, \frac{p_X(x_j)q(x_j \rightarrow x_i)}{p_X(x_i)q(x_i \rightarrow x_j)} \right) \quad (6)$$

$A(x_i \rightarrow x_j)$ represents the probability of accepting a move from x_i to x_j , ensuring that the sampling process converges to the target distribution p_X .

The algorithm then proceeds as follows: Starting from a randomly initialized state x_0 , MH generates a sequence of states $x_0 \rightarrow x_1 \rightarrow \dots \rightarrow x_T$. At each step, a new state x_j is sampled from current state x_i using the proposal distribution $q(x_i \rightarrow x_j)$. This proposal is then accepted with probability $A(x_i \rightarrow x_j)$, resulting in the next state being x_j , or rejected, resulting in the next state remaining x_i . If the proposal distribution q ensures that the state transitions are *ergodic*, MH is guaranteed to asymptotically converge to a sample drawn from the distribution p_X .

2.3.2. 3DGS Training with SGLD

MH algorithm can be used to draw a sample G from distribution p in Eq. 5 to obtain 3D Gaussian parameters. Starting from a random initial state G_0 , MH generates a sequence of transitions $G_0 \rightarrow G_1 \rightarrow G_2 \dots G_T$. The proposal distribution for transition from state G_t to G_{t+1} in the sequence is given by:

$$q(G_t \rightarrow G_{t+1}) = \mathcal{N} \left(G_t + \frac{\epsilon}{2} \nabla_G \log(p(G_t)), \epsilon I \right) \quad (7)$$

where \mathcal{N} is the standard normal distribution, ϵ is a step size parameter, $\nabla_G \log(p(G_t))$ is the gradient of the log-likelihood of the parameters given the ground truth images, and I is the identity matrix. In standard MH, an acceptance distribution $A(G_t \rightarrow G_{t+1})$ would be used to determine

whether to accept the proposed transition:

$$A(G_t \rightarrow G_{t+1}) = \min \left(1, \frac{p(G_{t+1})q(G_{t+1} \rightarrow G_t)}{p(G_t)q(G_t \rightarrow G_{t+1})} \right) \quad (8)$$

However, in the Stochastic Gradient Langevin Dynamics (SGLD) approximation, this explicit acceptance step is omitted. Specifically, the SGLD update rule is given by:

$$G_{t+1} = G_t + \frac{\epsilon}{2} \nabla_G \log(p(G_t)) + \sqrt{\epsilon} \eta \quad (9)$$

where $\eta \sim \mathcal{N}(0, I)$.

3. Related Work

Compressing Scenes Represented by 3DGS. A range of prior works [5–7, 10, 11, 18, 44, 46, 47, 55, 69, 70] aim to compress trained 3DGS models in order to reduce the storage required or to accelerate rendering speeds. To do this, these works propose several techniques such as pruning redundant gaussians, quantization, reducing bit-widths of less sensitive parameters, and cutting down higher order spherical harmonics coefficients to reduce the storage footprint needed to represent the scene. Other prior works [10, 31, 47] also propose using codebooks to compress the model memory footprint. However, these approaches compress the 3D model representation *post-training*. In this work, we aim to enable both, efficient training and rendering, by reducing the memory usage during the training process itself. To this end, we propose a novel codebook-based compression mechanism that significantly reduces memory utilization and model size during training.

Accelerating 3DGS Training. Prior works propose a range of techniques to accelerate 3DGS training. SpeedySplat [17], TurboGS [36], and TamingGS [39] propose densification control heuristic strategies to reduce the number of gaussians and thus accelerate both training and rendering. These approaches reduce the memory consumption during training, however they incur some loss in representation quality. We quantitatively compare against these works in Section 5, and we demonstrate that our approach achieves higher or similar compression rates without sacrificing representation quality.¹ Additionally, these approaches require careful tuning of the heuristic hyperparameters that may not generalize well across 3D scenes. EAGLES [15] and Scaffold-GS [37] aim to accelerate training speeds by using a compact representation that leverages neural networks to store 3D gaussian parameters more efficiently. We compare against EAGLES and Scaffold-GS in Section 5 and demonstrate that it cannot achieve the same representation quality as state-of-art approaches.

¹ We could not compare against TurboGS [36] due to lack of availability of open-source code, but would incur the same quality challenges due to the reduced number of Gaussians for representation.

Recent works such as 3DGS-LM [20] and 3DGS² [29] propose using second order optimization techniques that require fewer iterations for convergence, thus accelerating the training process. These approaches are orthogonal to our work and we note that 3DGS-LM only reports small speedups over the baseline [25]. Other works [8, 12, 33, 39] propose low-level optimizations to the renderer’s GPU code implementation or hardware support to speed up 3D gaussian splatting training [9, 30]. These training acceleration approaches are orthogonal to our work.

4. Method

Our goal in this work is to enable training *compressed representations* of 3D Gaussians for high-speed and memory efficient 3D reconstruction. To this end, we leverage codebook representations that can significantly reduce the amount of memory required to store 3DGS parameters. While codebooks have been demonstrated to be highly effective at compressing fully trained 3DGS models [10, 31, 47], directly *training* using codebook representations is an unsolved challenge. In this work, we solve the problem of learning on codebook-compressed representations by using MCMC sampling to sample over a posterior distribution of these compressed representations.

This requires (1) defining a state space for codebook-compressed 3DGS parameters; (2) formulating a posterior distribution over the codebook-based state representation whose samples accurately reconstruct the 3D scene; and (3) defining state transitions and deriving corresponding proposal and acceptance probabilities for MCMC sampling. We now describe these elements of our approach.

4.1. Compressed Model State Space

We use a codebook representation similar to C3DGS [47], but note that ContraGS can also use a different codebook implementation (see Section 2.2). We define the state of the codebook-compressed 3DGS model as: $S = \{G, C\}$:

$$G = \{g_1, g_2, g_3, \dots, g_N\} \quad C = \{SH, SR\} \quad (10)$$

In this expression, C comprises the 3DGS codebooks: SH and SR . The SH codebook stores vectors of spherical harmonics coefficients used to derive the view dependent color. The SR codebook contains vectors, where each vector stores the scaling and quaternion parameters for each Gaussian. G corresponds to the set of 3D Gaussians, where g_i corresponds to a Gaussian with the following parameters:

$$g_i = \{\mathbf{p}_i, o_i, g2sr_i, g2sh_i\} \quad (11)$$

Here, \mathbf{p}_i is the position of the mean, o_i the opacity. $g2sh$ and $g2sr$ are integers that are pointers to vectors in the SH and SR codebook respectively. Thus, a single 3D Gaussian in the compressed 3DGS model G is represented as $s_i =$

$\{g_i, C\}$. The state space representation described above is summarized in Fig. 4.

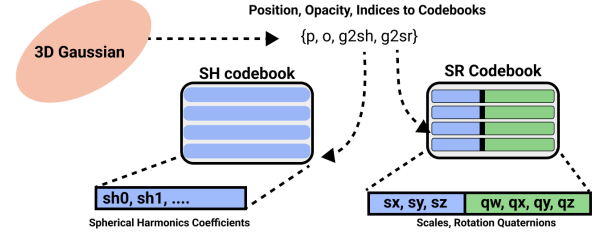


Figure 4. **Codebook layout used for ContraGS.** ContraGS allocates two codebooks: (1) SH stores spherical harmonics coefficients of RGB colors, and (2) SR stores scaling + quaternion parameters concatenated together as vectors. Each Gaussian has $g2sh, g2sr$ to index the two codebooks.

4.2. Formulating The Posterior Distribution

We define a posterior probability distribution over the ContraGS model state space as follows:

$$p(G, C) \propto \exp(-\mathcal{L}[I_{\mathcal{P}}(G, C), I_{\mathcal{P}}^{gt}]) \quad (12)$$

$I_{\mathcal{P}}(G, C)$ represents the image rendered from camera pose \mathcal{P} using the ContraGS codebook-based Gaussian model state (G, C) , and $I_{\mathcal{P}}^{gt}$ is the corresponding ground truth images. We define the reconstruction loss function \mathcal{L} as:

$$\mathcal{L} = \mathcal{L}_{\text{recon}} + \lambda_{sr}|SR| + \lambda_{sh}|SH| \quad (13)$$

$\mathcal{L}_{\text{recon}}$ is the reconstruction loss (defined in Eq. 4). The terms $|SR|$ and $|SH|$ represent the number of vectors in the SR and SH codebooks, respectively. λ_{sr} and λ_{sh} are hyperparameters used to control the size of these codebooks.

Bayesian inference over this probability function is performed by sampling the state $S = \{G, C\}$. Due to the high dimensionality of the distribution, we use MCMC sampling. However, unlike recent 3DGS-MCMC [26] that uses SGLD for MCMC sampling (see Section 2.3.2), SGLD cannot be applied to learn a discrete set of parameters such as the mapping/indexing between the Gaussians and codebook vectors. Instead we use the MH algorithm to sample from the posterior defined on codebook-compressed representations. To apply MH, we must define a proposal distribution and derive an acceptance distribution (see Section 2.3.1). The proposal distribution enables splitting and merging codebook vectors to transition between states with different mappings between Gaussians and codebook vectors. This allows MCMC to explore the joint space of continuous parameters. We now define the possible set of state transitions over codebook-based 3DGS representations, and define proposal distributions between these transitions.

4.3. Model State Space Transitions

To sample from the probability distribution in Eq. 12 using MH, we need to define a proposal and acceptance distribu-

tion functions (see Section 2.3.1). To do this, we first define a set of valid state transitions: (1) **parameter update**, (2) **merge** and (3) **split**.

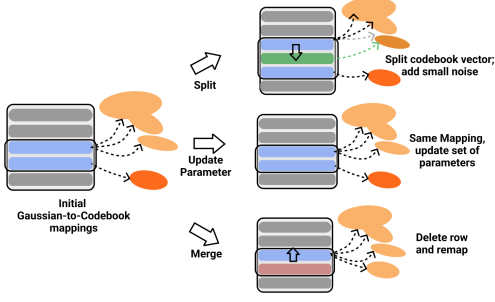
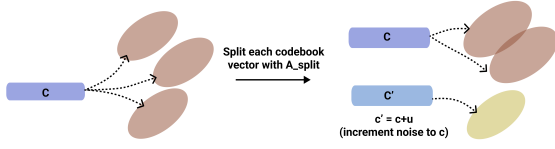
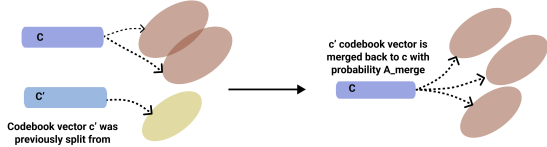


Figure 5. ContraGS performs one of the 3 steps for each 3DG: (1) Updates Gaussian and codebook parameters, or (2) Splitting the 3DG’s corresponding vector, or (3) Merge to the vector it previously split from.

- **Parameter Update:** This involves changing the values of the parameters of the SH, SR codebooks as well as 3D Gaussian parameters in g_i . The parameters are determined by the proposal distribution q_{update} . The mappings of the Gaussians to codebook vectors remains unchanged.
- **Split:** A Gaussian mapped to a codebook vector is split and allocated a new codebook vector, as shown in Fig. 6a. The 3D Gaussian mapped to codebook vector c is allocated a new codebook vector c' . The value of c' is generated by the proposal distribution q_{split} .
- **Merge:** A Gaussian mapping to a codebook vector c' can be merged with a codebook vector c from which it was previously split from, as shown in Fig. 6b. The parameters in the codebook vector are unchanged.



(a) Split transition: a codebook vector referred to by two or more 3D Gaussian parameter is split into two vectors.



(b) Merge transition: two codebook vectors referred to by different 3D Gaussian parameters gets merged into one.

Figure 6. Split and Merge transitions.

We now derive the proposal and acceptance distributions.

4.4. Proposal and Acceptance Distributions

We define the proposal distribution for MH sampling transition from state as:

$$q(S \rightarrow S') = 0.98q_{update} + 0.01q_{split} + 0.01q_{merge} \quad (14)$$

Where q_{update} is the parameter update transition, q_{split} is the split transition and q_{merge} is the merge transition. In other words, at each step, we randomly choose the parameter update step 98% of the times, and the split, merge transitions 1% of the time. Now, we define the proposal distributions for each type of transition, and derive the acceptance distributions as in Section 2.3.1. Please refer to Section A.1 in the Appendix for a detailed derivation.

Parameter update step The proposal distribution for a parameter update, q_{update} , is identical to the SGLD parameter update, as described in Section 2.3.2. Thus we express the parameter update state transition using q_{update} as follows:

$$q_{update}(S_{diff}) = \mathcal{N}\left(S_{diff} + \frac{\epsilon_p}{2} \nabla_{S_{diff}} \log(p(S)), \epsilon_p I\right) \quad (15)$$

Where ϵ_p is a small hyperparameters. S_{diff} is the differentiable set of parameters (all parameters except the indices to the codebooks). The update step is equivalent to the SGLD update step with acceptance $A = 1$.

Split Step: During the split transition, for each Gaussian, we allocate a new codebook vector and remap. A Gaussian mapped to codebook vector c is remapped to a new codebook vector entry row c'' . The original codebook vector becomes c' .

$$c' = c \quad c'' = c + u \quad (16)$$

$$q_{split}(u) = \mathcal{N}(u | \mu = 0, \sigma = \epsilon_{split} I) \quad (17)$$

Where ϵ_{split} is a hyperparameter.

Merge Step: Two codebook vectors c, c' can be merged into one codebook vector of value c . Two rows to be merged are selected with a transition distribution defined by:

$$q_{merge}(S \rightarrow S_{merge}) = \mathcal{N}(c - c' | \mu = 0, \sigma = \epsilon_{merge} I) \quad (18)$$

Where ϵ_{merge} is a hyperparameter.

Acceptance: Acceptance probabilities of the split and merge step can be derived as:

$$A(S \rightarrow S_{split}) = \min\left(1, e^{-\lambda_{SH}} \frac{1}{q_{sm}(c' - c'')}\right) \quad (19)$$

$$A(S \rightarrow S_{merge}) = \min\left(1, e^{\lambda_{SH}} q_{sm}(c - c')\right) \quad (20)$$

Where q_{sm} is given by:

$$q_{sm}(u) = \exp\left(\frac{-u^2}{2} \left(\frac{1}{\epsilon_{split}^2} - \frac{1}{\epsilon_{merge}^2}\right)\right) \quad (21)$$

5. Results

5.1. Experiment Setup

Evaluation Platform, Hyperparameter Configuration.

We measure training and rendering speeds of ContraGS on a

	MipNerf360				Deep Blending				Tanks and Temples			
	PSNR	SSIM	LPIPS	Peak Mem	PSNR	SSIM	LPIPS	Peak Mem	PSNR	SSIM	LPIPS	Peak Mem
3DGS*	29.09	0.867	0.183	2089.363	30.10	0.909	0.241	817.159	22.03	0.821	0.197	901.405
EAGLES*	28.70	0.867	0.194	159.473	30.38	0.913	0.251	159.473	22.34	0.798	0.237	57.962
SpeedySplat*	28.33	0.846	0.241	-	30.02	0.907	0.269	-	21.68	0.773	0.289	-
Reduced-GS*	29.03	0.870	0.184	1432.407	29.96	0.906	0.243	572.136	23.72	0.846	0.176	636.500
Taming-GS*	29.39	0.863	0.198	477.598	30.11	0.910	0.251	325.629	22.58	0.830	0.191	1189.745
Scaffold-GS*	29.22	0.869	0.190	304.827	30.89	0.913	0.244	95.107	22.54	0.829	0.190	192.211
MCMC-2M	30.71	0.908	0.161	473.000	33.99	0.929	0.243	473.000	24.32	0.864	0.182	473.000
Ours-2M	30.06	0.899	0.175	130.038	33.73	0.925	0.252	120.672	24.35	0.861	0.187	127.968
MCMC-5M	32.72	0.943	0.128	1182.000	34.54	0.939	0.209	1182.000	26.63	0.911	0.112	1182.000
Ours-5M	31.01	0.919	0.146	275.594	34.33	0.932	0.232	444.259	26.18	0.898	0.127	338.000

Table 1. Averaged PSNR, SSIM and LPIPS and peak model memory during training (SfM initialization for * approaches)

system with a Core i7-13700K CPU and an NVIDIA RTX-4090 GPU. For our evaluation, we set λ_{SH} to 2.3, $\lambda_{SR} = 3$. ϵ_{split} and ϵ_{merge} are set to 0.1, 0.05 for both SH and SR codebooks. At each training step, we choose to perform the parameter update step with a probability of 98%, and the split and merge transitions with a 1% probability. We initialize training with 100000 Gaussians with random parameters and grow the number of Gaussians by 5% every 100 training iterations. We evaluate two versions of ContraGS, ContraGS-2M and ContraGS-5M in which we cap the Gaussians count at 2 million and 5 million respectively. **Dataset and Metrics.** We evaluate ContraGS on 3D reconstruction tasks using multi-view images. We measure the PSNR, LPIPS and SSIM on evaluation views of 3D reconstruction tasks. We consider the following datasets that contain multiview images of real world and synthetic 3D scenes: MipNerf360 [2] (counter, stump, kitchen, bicycle, bonsai, room and garden scenes), Blender [41] (chair, drums, ficus, hotdog, lego, materials, mic and ship scenes), Deep Blending’s Playroom scene and Tanks and Temples [27] (Truck and Train scenes) datasets.

Prior Work Comparisons. We then compare the reconstruction quality with prior works. We compare ContraGS approach against 3DGS [25], MCMC-2M [26], and MCMC-5M (two configurations with 2 million and 5 million Gaussians respectively); 3DGS-MCMC [26] achieves state-of-art representation quality. Both MCMC-5M and ContraGS-5M incur higher memory cost than their respective 2M configurations but provide higher representation qualities. We also compare with other prior works that enable faster and more memory efficient training by pruning the number of Gaussians (Section 3): EAGLES [15], SpeedySplat [17], Reduced-GS[46], TamingGS [39], Scaffold-GS [37]. For prior work, we initialize the positions and RGB colors of the Gaussians using the corresponding Structure-from-Motion point cloud.

5.2. Representation Quality & Peak Model Memory

Table 1 shows the average PSNR, SSIM, LPIPS and the peak model memory during training (in MB) achieved by ContraGS on multiview 3D scene reconstruction tasks. PSNR, SSIM and LPIPS measured for individual scenes are

presented in Section B of Appendix along with qualitative comparisons of generated images.

First, we observe that ContraGS is able to achieve similar representation quality as that of a state-of-art approach 3DGS-MCMC [26]: less than 0.3 PSNR on average with 2 million Gaussians, and less than 0.8 PSNR on average with 5 million Gaussians. ContraGS-2M achieves PSNR equivalent to MCMC-2M on the Deep Blending and Tanks and Temples datasets, and incurs a 0.65 PSNR drop on average on the MipNerf360 dataset. ContraGS-5M also achieves equivalent PSNR on the DeepBlending incurs a sharper PSNR drop on MipNerf360 (1.5 PSNR). At the same time, ContraGS requires significantly less peak model memory ($3.78\times$ and $3.5\times$ on average respectively). Second, ContraGS-5M outperforms MCMC-2M on all quality metrics (PSNR, SSIM and LPIPS) while having smaller model memory size ($1.39\times$ on average). Third, compared to the prior work that aims to achieve memory efficient training, ContraGS-2M achieves significantly higher representation quality while having a similar peak memory usage compared to EAGLES, Reduced-GS, Taming-GS and Scaffold-GS. Finally, compared to 3DGS, ContraGS-2M is able to significantly reduce the peak model memory during training, by $9.99\times$ on average. We conclude that ContraGS enables significantly reduced peak memory during training while retaining close to state-of-art quality. Thus, for any memory capacity constraint (i.e, peak memory utilization), ContraGS achieves the highest representation quality compared to prior works.

Random point cloud initialization. We note that ContraGS-2M and ContraGS-5M (and MCMC-2M, 5M) are able to reconstruct the scene initialized on a random point cloud). The results presented in this section for these configurations are with randomly initialized Gaussian parameters. EAGLES, Taming-GS, SpeedySplat, Reduced-GS require the SfM point cloud to initialize the Gaussian parameters and the results in this section were collected using SfM. A fairer comparison between these methods would assume a random initialization, but since certain scenes in the MipNerf360, Deep Blending, Tanks and Temples datasets could not be trained with random initialization for these approaches, the results in Table 1 include SfM ini-

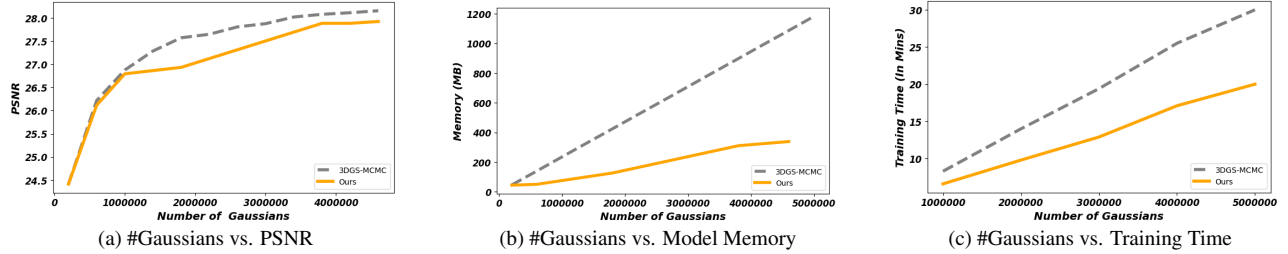


Figure 7. The impact of Gaussian count for 3DGS-MCMC and ContraGS on training quality (PSNR), model memory, and training time.

tialization for all approaches except ContraGS and MCMC. We were able to train scenes in the Blender dataset for all approaches (except Taming-GS) with random initialization, and we present these results in Table 2.

Table 2 shows the average quality metrics and peak memory during training of ContraGS-2M for synthetic scenes in the Blender dataset. ContraGS-2M achieves a significantly higher reconstruction quality compared to prior works. Although the peak model memory during training of ContraGS-2M is higher in comparison, the peak memory is in the same range as that of real world scenes in Table 1. We do not report results from MCMC here because MCMC-2M fails to reconstruct all synthetic scenes when setting the Gaussians count to 2M, due to instability in the training process.

	PSNR	SSIM	LPIPS	Peak Mem
3DGS	31.07	0.959	0.051	83.00
EAGLES	32.55	0.964	0.039	5.17
SpeedySplat	32.43	0.960	0.050	47.89
Reduced-GS	33.80	0.970	0.030	49.72
Scaffold-GS	33.46	0.967	0.034	31.66
Ours-2M	36.840	0.984	0.023	257.87

Table 2. PSNR, SSIM, LPIPS for different workloads on the Blender dataset (GS parameters initialized randomly)

5.3. Training and Rendering Speeds

Table 3 shows the average training speed in terms of training iterations per second for ContraGS. We observe that, when compared to MCMC-2M, ContraGS-2M is able to speed up training and rendering by $1.36\times$ and $1.88\times$ on average. We also compare against Taming3DGS, the state-of-art for efficient training, in Section E of the Appendix. These works achieve higher training and rendering speeds. However, the representation quality is significantly lower.

	MipNerf360		Deep Blending		T & T	
	Train It/s	FPS	Train It/s	FPS	Train It/s	FPS
MCMC	23.65	102	31.66	161	30.34	133
Ours	32.02	216	46.33	319	40.75	207
MCMC-5M	11.71	65	14.06	114	12.95	80
Ours-5M	21.1	87	19.87	141	19.18	114

Table 3. Training and rendering speeds

5.4. Ablation Study

Quality vs. Gaussians Count. Figure 7a depicts the PSNR achieved by ContraGS and 3DGS-MCMC on varying the number of Gaussians used to represent the Truck scene of the T&T dataset. We observe that as the Gaussian count increases, the PSNR achieved by ContraGS incurs a small degradation in quality compared to 3DGS-MCMC. At 5 million Gaussians, the difference in PSNR is about 0.46 on average. Similar to 3DGS-MCMC, ContraGS achieves higher representation quality with a greater Gaussian count.

Model memory vs. Number of Gaussians. Fig. 7b depicts how the post-training memory footprint of the model varies with the Gaussians count for the Tanks and Temples dataset. This memory footprint increases linearly with the Gaussian count for 3DGS-MCMC. However, ContraGS is able to represent large Gaussian counts without significantly increasing the memory footprint and requires a lot less memory than 3DGS-MCMC ($3.49\times$ on average).

Training speed vs. Number of Gaussians. Fig. 7c depicts the wall clock time needed to train the playroom scene of the Deep Blending dataset for 30000 iterations. With 3DGS-MCMC, the training time increases linearly with the gaussian count, however, ContraGS enable more efficient and scalable training at larger gaussian counts.

6. Conclusion

We introduce ContraGS, a novel method for learning codebook-compressed representations of 3D Gaussian Splatting for high-speed memory-efficient scene reconstruction. ContraGS can effectively reduce the model’s memory footprint during training while accelerating training and rendering. This makes ContraGS useful for reconstructing complex scenes with 3DGS, which is challenging on resource-constrained platforms such as mobile devices and web browsers. ContraGS achieves the highest representation quality for any memory capacity constraint (i.e, peak memory utilization) compared to existing approaches. ContraGS provides an extensible mathematical framework that can be applied to do compressed training on a range of point-based scene representation methods.

References

- [1] Jad Abou-Chakra, Krishan Rana, Feras Dayoub, and Niko Sünderhauf. Physically embodied gaussian splatting: A real-time correctable world model for robotics. *arXiv preprint arXiv:2406.10788*, 2024. 2
- [2] Jonathan T Barron, Ben Mildenhall, Dor Verbin, Pratul P Srinivasan, and Peter Hedman. Mip-nerf 360: Unbounded anti-aliased neural radiance fields. In *Proceedings of the IEEE/CVF conference on computer vision and pattern recognition*, pages 5470–5479, 2022. 7
- [3] Minghao Chen, Iro Laina, and Andrea Vedaldi. Dge: Direct gaussian 3d editing by consistent multi-view editing. In *European Conference on Computer Vision*, pages 74–92. Springer, 2024. 2
- [4] Yiwen Chen, Zilong Chen, Chi Zhang, Feng Wang, Xiaofeng Yang, Yikai Wang, Zhongang Cai, Lei Yang, Huaping Liu, and Guosheng Lin. Gaussianeditor: Swift and controllable 3d editing with gaussian splatting. In *Proceedings of the IEEE/CVF conference on computer vision and pattern recognition*, pages 21476–21485, 2024. 2
- [5] Yihang Chen, Qianyi Wu, Weiyao Lin, Mehrtash Harandi, and Jianfei Cai. Hac: Hash-grid assisted context for 3d gaussian splatting compression. In *European Conference on Computer Vision*, pages 422–438. Springer, 2024. 4
- [6] Yihang Chen, Qianyi Wu, Weiyao Lin, Mehrtash Harandi, and Jianfei Cai. Hac++: Towards 100x compression of 3d gaussian splatting. *arXiv preprint arXiv:2501.12255*, 2025.
- [7] Tianchen Deng, Yaohui Chen, Leyan Zhang, Jianfei Yang, Shenghai Yuan, Jiuming Liu, Danwei Wang, Hesheng Wang, and Weidong Chen. Compact 3d gaussian splatting for dense visual slam. *arXiv preprint arXiv:2403.11247*, 2024. 2, 4
- [8] Sankeerth Durvasula, Adrian Zhao, Fan Chen, Ruofan Liang, Pawan Kumar Sanjaya, and Nandita Vijaykumar. Distwar: Fast differentiable rendering on raster-based rendering pipelines. *arXiv preprint arXiv:2401.05345*, 2023. 5
- [9] Sankeerth Durvasula, Adrian Zhao, Fan Chen, Ruofan Liang, Pawan Kumar Sanjaya, Yushi Guan, Christina Gianoulas, and Nandita Vijaykumar. Arc: Warp-level adaptive atomic reduction in gpus to accelerate differentiable rendering. In *Proceedings of the 30th ACM International Conference on Architectural Support for Programming Languages and Operating Systems, Volume 1*, pages 64–83, 2025. 5
- [10] Zhiwen Fan, Kevin Wang, Kairun Wen, Zehao Zhu, Dejia Xu, Zhangyang Wang, et al. Lightgaussian: Unbounded 3d gaussian compression with 15x reduction and 200+ fps. *Advances in neural information processing systems*, 37: 140138–140158, 2025. 2, 4, 5
- [11] Guangchi Fang and Bing Wang. Mini-splatting: Representing scenes with a constrained number of gaussians. In *European Conference on Computer Vision*, pages 165–181. Springer, 2024. 4
- [12] Guofeng Feng, Siyan Chen, Rong Fu, Zimu Liao, Yi Wang, Tao Liu, Zhilin Pei, Hengjie Li, Xingcheng Zhang, and Bo Dai. Flashgs: Efficient 3d gaussian splatting for large-scale and high-resolution rendering. *arXiv preprint arXiv:2408.07967*, 2024. 5
- [13] Quankai Gao, Qiangeng Xu, Zhe Cao, Ben Mildenhall, Wenchao Ma, Le Chen, Danhang Tang, and Ulrich Neumann. Gaussianflow: Splatting gaussian dynamics for 4d content creation. *arXiv preprint arXiv:2403.12365*, 2024. 2
- [14] Ruiqi Gao, Aleksander Holynski, Philipp Henzler, Arthur Brussee, Ricardo Martin-Brualla, Pratul Srinivasan, Jonathan T Barron, and Ben Poole. Cat3d: Create anything in 3d with multi-view diffusion models. *arXiv preprint arXiv:2405.10314*, 2024. 2
- [15] Sharath Girish, Kamal Gupta, and Abhinav Shrivastava. Eagles: Efficient accelerated 3d gaussians with lightweight encodings. In *European Conference on Computer Vision*, pages 54–71. Springer, 2024. 2, 4, 7
- [16] Shrisudhan Govindarajan, Daniel Rebain, Kwang Moo Yi, and Andrea Tagliasacchi. Radiant foam: Real-time differentiable ray tracing. *arXiv preprint arXiv:2502.01157*, 2025. 3
- [17] Alex Hanson, Allen Tu, Geng Lin, Vasu Singla, Matthias Zwicker, and Tom Goldstein. Speedy-splat: Fast 3d gaussian splatting with sparse pixels and sparse primitives. *arXiv preprint arXiv:2412.00578*, 2024. 2, 4, 7
- [18] Alex Hanson, Allen Tu, Vasu Singla, Mayuka Jayawardhana, Matthias Zwicker, and Tom Goldstein. Pup 3d-gs: Principled uncertainty pruning for 3d gaussian splatting. *arXiv preprint arXiv:2406.10219*, 2024. 2, 4
- [19] W. K. Hastings. Monte carlo sampling methods using markov chains and their applications. *Biometrika*, 57(1):97–109, 1970. 4
- [20] Lukas Höllein, Aljaž Božič, Michael Zollhöfer, and Matthias Nießner. 3dgs-lm: Faster gaussian-splatting optimization with levenberg-marquardt. *arXiv preprint arXiv:2409.12892*, 2024. 5
- [21] Jiarui Hu, Xianhao Chen, Boyin Feng, Guanglin Li, Liangjing Yang, Hujun Bao, Guofeng Zhang, and Zhaopeng Cui. Cg-slam: Efficient dense rgb-d slam in a consistent uncertainty-aware 3d gaussian field. In *European Conference on Computer Vision*, pages 93–112. Springer, 2024. 2
- [22] Yue Hu, Rong Liu, Meida Chen, Andrew Feng, and Peter Beerel. Splatmap: Online dense monocular slam with 3d gaussian splatting. *arXiv preprint arXiv:2501.07015*, 2025. 2
- [23] Lutao Jiang, Xu Zheng, Yuanhuiyi Lyu, Jiazhou Zhou, and Lin Wang. Brightdreamer: Generic 3d gaussian generative framework for fast text-to-3d synthesis. *arXiv preprint arXiv:2403.11273*, 2024. 2
- [24] HyunJun Jung, Nikolas Brasch, Jifei Song, Eduardo Perez-Pellitero, Yiren Zhou, Zhihao Li, Nassir Navab, and Benjamin Busam. Deformable 3d gaussian splatting for animatable human avatars. *arXiv preprint arXiv:2312.15059*, 2023. 2
- [25] Bernhard Kerbl, Georgios Kopanas, Thomas Leimkühler, and George Drettakis. 3d gaussian splatting for real-time radiance field rendering. *ACM Trans. Graph.*, 42(4):139–1, 2023. 1, 3, 5, 7
- [26] Shakiba Kheradmand, Daniel Rebain, Gopal Sharma, Weiwei Sun, Jeff Tseng, Hossam Isack, Abhishek Kar, Andrea Tagliasacchi, and Kwang Moo Yi. 3d gaussian

- splatting as markov chain monte carlo. *arXiv preprint arXiv:2404.09591*, 2024. 2, 3, 5, 7
- [27] Arno Knapitsch, Jaesik Park, Qian-Yi Zhou, and Vladlen Koltun. Tanks and temples: Benchmarking large-scale scene reconstruction. *ACM Transactions on Graphics*, 36(4), 2017. 2, 7
- [28] Muhammed Kocabas, Jen-Hao Rick Chang, James Gabriel, Oncel Tuzel, and Anurag Ranjan. Hugs: Human gaussian splats. In *Proceedings of the IEEE/CVF conference on computer vision and pattern recognition*, pages 505–515, 2024. 2
- [29] Lei Lan, Tianjia Shao, Zixuan Lu, Yu Zhang, Chenfanfu Jiang, and Yin Yang. 3dgs²: Near second-order converging 3d gaussian splatting. *arXiv preprint arXiv:2501.13975*, 2025. 5
- [30] Junseo Lee, Seokwon Lee, Jungi Lee, Junyong Park, and Jaewoong Sim. Gscore: Efficient radiance field rendering via architectural support for 3d gaussian splatting. In *Proceedings of the 29th ACM International Conference on Architectural Support for Programming Languages and Operating Systems, Volume 3*, pages 497–511, 2024. 5
- [31] Joo Chan Lee, Daniel Rho, Xiangyu Sun, Jong Hwan Ko, and Eunbyung Park. Compact 3d gaussian representation for radiance field. In *Proceedings of the IEEE/CVF Conference on Computer Vision and Pattern Recognition*, pages 21719–21728, 2024. 2, 4, 5
- [32] Xinhai Li, Jialin Li, Ziheng Zhang, Rui Zhang, Fan Jia, Tiancai Wang, Haoqiang Fan, Kuo-Kun Tseng, and Ruiping Wang. Robogsim: A real2sim2real robotic gaussian splatting simulator. *arXiv preprint arXiv:2411.11839*, 2024. 2
- [33] Weikai Lin, Yu Feng, and Yuhao Zhu. Rtgs: Enabling real-time gaussian splatting on mobile devices using efficiency-guided pruning and foveated rendering. *arXiv preprint arXiv:2407.00435*, 2024. 5
- [34] Rong Liu, Rui Xu, Yue Hu, Meida Chen, and Andrew Feng. Atomgs: Atomizing gaussian splatting for high-fidelity radiance field. *arXiv preprint arXiv:2405.12369*, 2024. 2
- [35] Rong Liu, Dylan Sun, Meida Chen, Yue Wang, and Andrew Feng. Deformable beta splatting. *arXiv preprint arXiv:2501.18630*, 2025. 3
- [36] Tao Lu, Ankit Dhiman, R Srinath, Emre Arslan, Angela Xing, Yuanbo Xiangli, R Venkatesh Babu, and Srinath Sridhar. Turbo-gs: Accelerating 3d gaussian fitting for high-quality radiance fields. *arXiv preprint arXiv:2412.13547*, 2024. 2, 4
- [37] Tao Lu, Mulin Yu, Linning Xu, Yuanbo Xiangli, Limin Wang, Dahua Lin, and Bo Dai. Scaffold-gs: Structured 3d gaussians for view-adaptive rendering. In *Proceedings of the IEEE/CVF Conference on Computer Vision and Pattern Recognition*, pages 20654–20664, 2024. 4, 7
- [38] Tao Lu, Mulin Yu, Linning Xu, Yuanbo Xiangli, Limin Wang, Dahua Lin, and Bo Dai. Scaffold-gs: Structured 3d gaussians for view-adaptive rendering. In *Proceedings of the IEEE/CVF Conference on Computer Vision and Pattern Recognition*, pages 20654–20664, 2024. 2
- [39] Saswat Subhrajyoti Mallick, Rahul Goel, Bernhard Kerbl, Markus Steinberger, Francisco Vicente Carrasco, and Fernando De La Torre. Taming 3dgs: High-quality radiance fields with limited resources. In *SIGGRAPH Asia 2024 Conference Papers*, pages 1–11, 2024. 4, 5, 7
- [40] Marko Mihajlovic, Sergey Prokudin, Siyu Tang, Robert Maier, Federica Bogo, Tony Tung, and Edmond Boyer. Splatfields: Neural gaussian splats for sparse 3d and 4d reconstruction. In *European Conference on Computer Vision*, pages 313–332. Springer, 2024. 2
- [41] Ben Mildenhall, Pratul P Srinivasan, Matthew Tancik, Jonathan T Barron, Ravi Ramamoorthi, and Ren Ng. Nerf: Representing scenes as neural radiance fields for view synthesis. *Communications of the ACM*, 65(1):99–106, 2021. 7
- [42] Gyeongsik Moon, Takaaki Shiratori, and Shunsuke Saito. Expressive whole-body 3d gaussian avatar. In *European Conference on Computer Vision*, pages 19–35. Springer, 2024. 2
- [43] Arthur Moreau, Jifei Song, Helisa Dharmo, Richard Shaw, Yiren Zhou, and Eduardo Pérez-Pellitero. Human gaussian splatting: Real-time rendering of animatable avatars. In *Proceedings of the IEEE/CVF conference on computer vision and pattern recognition*, pages 788–798, 2024. 2
- [44] Michael Niemeyer, Fabian Manhardt, Marie-Julie Rakotsasona, Michael Oechsle, Daniel Duckworth, Rama Gosula, Keisuke Tateno, John Bates, Dominik Kaeser, and Federico Tombari. Radsplat: Radiance field-informed gaussian splatting for robust real-time rendering with 900+ fps. *arXiv preprint arXiv:2403.13806*, 2024. 4
- [45] Francesco Palandra, Andrea Sanchietti, Daniele Baieri, and Emanuele Rodolà. Gsedit: Efficient text-guided editing of 3d objects via gaussian splatting. *arXiv preprint arXiv:2403.05154*, 2024. 2
- [46] Panagiotis Papantonakis, Georgios Kopanas, Bernhard Kerbl, Alexandre Lanvin, and George Drettakis. Reducing the memory footprint of 3d gaussian splatting. *Proceedings of the ACM on Computer Graphics and Interactive Techniques*, 7(1):1–17, 2024. 4, 7
- [47] Jiating Qian, Yiming Yan, Fengjiao Gao, Baoyu Ge, Maosheng Wei, Boyi Shangguan, and Guangjun He. C3dgs: Compressing 3d gaussian model for surface reconstruction of large-scale scenes based on multi-view uav images. *IEEE Journal of Selected Topics in Applied Earth Observations and Remote Sensing*, 2025. 2, 3, 4, 5
- [48] Zhiyin Qian, Shaofei Wang, Marko Mihajlovic, Andreas Geiger, and Siyu Tang. 3dgs-avatar: Animatable avatars via deformable 3d gaussian splatting. In *Proceedings of the IEEE/CVF conference on computer vision and pattern recognition*, pages 5020–5030, 2024. 2
- [49] Yansong Qu, Dian Chen, Xinyang Li, Xiaofan Li, Shengchuan Zhang, Liujuan Cao, and Rongrong Ji. Drag your gaussian: Effective drag-based editing with score distillation for 3d gaussian splatting. *arXiv preprint arXiv:2501.18672*, 2025. 2
- [50] Darius Rückert, Linus Franke, and Marc Stamminger. Adop: Approximate differentiable one-pixel point rendering. *ACM Transactions on Graphics (ToG)*, 41(4):1–14, 2022. 3
- [51] Zhijing Shao, Zhaolong Wang, Zhuang Li, Duotun Wang, Xiangru Lin, Yu Zhang, Mingming Fan, and Zeyu Wang.

- Splattingavatar: Realistic real-time human avatars with mesh-embedded gaussian splatting. In *Proceedings of the IEEE/CVF Conference on Computer Vision and Pattern Recognition*, pages 1606–1616, 2024. [2](#)
- [52] David Svitov, Pietro Morerio, Lourdes Agapito, and Alessio Del Bue. Haha: Highly articulated gaussian human avatars with textured mesh prior. In *Proceedings of the Asian Conference on Computer Vision*, pages 4051–4068, 2024. [2](#)
- [53] Jiayang Tang, Jiawei Ren, Hang Zhou, Ziwei Liu, and Gang Zeng. Dreamgaussian: Generative gaussian splatting for efficient 3d content creation. *arXiv preprint arXiv:2309.16653*, 2023. [2](#)
- [54] Nicolas von Lützwow and Matthias Nießner. Linprim: Linear primitives for differentiable volumetric rendering. *arXiv preprint arXiv:2501.16312*, 2025. [3](#)
- [55] Henan Wang, Hanxin Zhu, Tianyu He, Runsen Feng, Jiajun Deng, Jiang Bian, and Zhibo Chen. End-to-end rate-distortion optimized 3d gaussian representation. In *European Conference on Computer Vision*, pages 76–92. Springer, 2024. [2](#), [4](#)
- [56] Guanjun Wu, Taoran Yi, Jiemin Fang, Lingxi Xie, Xiaopeng Zhang, Wei Wei, Wenyu Liu, Qi Tian, and Xinggang Wang. 4d gaussian splatting for real-time dynamic scene rendering. In *Proceedings of the IEEE/CVF conference on computer vision and pattern recognition*, pages 20310–20320, 2024. [2](#)
- [57] Jing Wu, Jia-Wang Bian, Xinghui Li, Guangrun Wang, Ian Reid, Philip Torr, and Victor Adrian Prisacariu. Gaussctrl: Multi-view consistent text-driven 3d gaussian splatting editing. In *European Conference on Computer Vision*, pages 55–71. Springer, 2024. [2](#)
- [58] Tianyi Xie, Zeshun Zong, Yuxing Qiu, Xuan Li, Yutao Feng, Yin Yang, and Chenfanfu Jiang. Physgaussian: Physics-integrated 3d gaussians for generative dynamics. In *Proceedings of the IEEE/CVF Conference on Computer Vision and Pattern Recognition*, pages 4389–4398, 2024. [2](#)
- [59] Xinli Xu, Wenhong Ge, Dicong Qiu, ZhiFei Chen, Dongyu Yan, Zhuoyun Liu, Haoyu Zhao, Hanfeng Zhao, Shunsi Zhang, Junwei Liang, et al. Gaussianproperty: Integrating physical properties to 3d gaussians with Imms. *arXiv preprint arXiv:2412.11258*, 2024. [2](#)
- [60] Yueming Xu, Haochen Jiang, Zhongyang Xiao, Jianfeng Feng, and Li Zhang. Dg-slam: Robust dynamic gaussian splatting slam with hybrid pose optimization. *arXiv preprint arXiv:2411.08373*, 2024. [2](#)
- [61] Yansong Xu, Junlin Li, Wei Zhang, Siyu Chen, Shengyong Zhang, Yuquan Leng, and Weijia Zhou. Fgs-slam: Fourier-based gaussian splatting for real-time slam with sparse and dense map fusion. *arXiv preprint arXiv:2503.01109*, 2025.
- [62] Chi Yan, Delin Qu, Dan Xu, Bin Zhao, Zhigang Wang, Dong Wang, and Xuelong Li. Gs-slam: Dense visual slam with 3d gaussian splatting. In *Proceedings of the IEEE/CVF Conference on Computer Vision and Pattern Recognition*, pages 19595–19604, 2024. [2](#)
- [63] Ziyang Yan, Lei Li, Yihua Shao, Siyu Chen, Wuzong Kai, Jenq-Neng Hwang, Hao Zhao, and Fabio Remondino. 3dsce-needitor: Controllable 3d scene editing with gaussian splatting. *arXiv preprint arXiv:2412.01583*, 2024. [2](#)
- [64] Ziyi Yang, Xinyu Gao, Wen Zhou, Shaohui Jiao, Yuqing Zhang, and Xiaogang Jin. Deformable 3d gaussians for high-fidelity monocular dynamic scene reconstruction. In *Proceedings of the IEEE/CVF conference on computer vision and pattern recognition*, pages 20331–20341, 2024. [2](#)
- [65] Mingqiao Ye, Martin Danelljan, Fisher Yu, and Lei Ke. Gaussian grouping: Segment and edit anything in 3d scenes. In *European Conference on Computer Vision*, pages 162–179. Springer, 2024. [2](#)
- [66] Ye Yuan, Xueting Li, Yangyi Huang, Shalini De Mello, Koki Nagano, Jan Kautz, and Umar Iqbal. Avatar: Animatable 3d gaussian avatars with implicit mesh learning. In *Proceedings of the IEEE/CVF Conference on Computer Vision and Pattern Recognition*, pages 896–905, 2024. [2](#)
- [67] Dongbin Zhang, Chuming Wang, Weitao Wang, Peihao Li, Minghan Qin, and Haoqian Wang. Gaussian in the wild: 3d gaussian splatting for unconstrained image collections. In *European Conference on Computer Vision*, pages 341–359. Springer, 2024. [2](#)
- [68] Kai Zhang, Sai Bi, Hao Tan, Yuanbo Xiangli, Nanxuan Zhao, Kalyan Sunkavalli, and Zexiang Xu. Gs-lrm: Large reconstruction model for 3d gaussian splatting. In *European Conference on Computer Vision*, pages 1–19. Springer, 2024. [2](#)
- [69] Xinjie Zhang, Xingtong Ge, Tongda Xu, Dailan He, Yan Wang, Hongwei Qin, Guo Lu, Jing Geng, and Jun Zhang. Gaussianimage: 1000 fps image representation and compression by 2d gaussian splatting. In *European Conference on Computer Vision*, 2024. [4](#)
- [70] Zhaoliang Zhang, Tianchen Song, Yongjae Lee, Li Yang, Cheng Peng, Rama Chellappa, and Deliang Fan. Lp-3dgs: Learning to prune 3d gaussian splatting. *Advances in Neural Information Processing Systems*, 37:122434–122457, 2025. [4](#)
- [71] Hongliang Zhong, Can Wang, Jingbo Zhang, and Jing Liao. Generative object insertion in gaussian splatting with a multi-view diffusion model. *arXiv preprint arXiv:2409.16938*, 2024. [2](#)

A. Acceptance Probability Derivation

A.1. Proposal and Acceptance Probabilities

To determine whether a split, merge or parameter update step proposed is accepted to be taken or not - we compute the acceptance probability as follows:

$$A(S \rightarrow S') = \min \left(1, \frac{P(S')q(S|S')}{P(S)q(S'|S)} \right) \quad (22)$$

For the parameter update transition that uses the SGLD update, $A = 1$. For the merge and split transitions, the acceptance probability is given by:

$$A(S \rightarrow S_{\text{merge}}) = \min \left(1, \frac{P(S_{\text{merge}})q_{\text{split}}(S_{\text{merge}} \rightarrow S)}{P(S)q_{\text{merge}}(S \rightarrow S_{\text{merge}})} \right) \quad (23)$$

$$A(S \rightarrow S_{\text{split}}) = \min \left(1, \frac{P(S_{\text{split}})q_{\text{merge}}(S_{\text{split}} \rightarrow S)}{P(S)q_{\text{split}}(S \rightarrow S_{\text{split}})} \right) \quad (24)$$

We now derive the acceptance distribution.

A.1.1. Parameter update choice

The proposal distribution for a parameter update, q_{update} , is identical to the SGLD parameter update. Thus we express the parameter update state transition using q_{update} as follows:

$$\mathbf{p}_{t+1} \sim \mathcal{N} \left(\mathbf{p}_t + \frac{\epsilon_p}{2} \nabla_p \log(p(S)), \epsilon_p I \right) \quad (25)$$

$$\mathbf{o}_{t+1} \sim \mathcal{N} \left(\mathbf{o}_t + \frac{\epsilon_o}{2} \nabla_o \log(p(S)), \epsilon_o I \right) \quad (26)$$

$$\text{SH}_{t+1} \sim \mathcal{N} \left(\text{SH}_t + \frac{\epsilon_{\text{SH}}}{2} \nabla_{\text{SH}} \log(p(G, C)), \epsilon_{\text{SH}} I \right) \quad (27)$$

$$\text{SR}_{t+1} \sim \mathcal{N} \left(\text{SR}_t + \frac{\epsilon_{\text{SR}}}{2} \nabla_{\text{SR}} \log(p(G, C)), \epsilon_{\text{SR}} I \right) \quad (28)$$

Where $\epsilon_p, \epsilon_o, \epsilon_{\text{SH}}, \epsilon_{\text{SR}}$ are small hyperparameters. The acceptance probability $A = 1$.

A.1.2. Split Codebook Vectors

During the split transition, we split its codebook vector into a new entry. A 3DG mapped to codebook vector c is remapped into a new codebook vector entry row c'' . The original codebook vector becomes c' .

$$c' = c \quad c'' = c + u \quad (29)$$

$$q_{\text{split}}(u) = \mathcal{N}(0, \epsilon_{\text{split}} I) \quad (30)$$

The acceptance probability of this state transition is given by:

$$A(S \rightarrow S_{\text{split}}) = \min \left(1, \frac{p(S_{\text{split}})q_{\text{merge}}(c - c')}{p(S)q_{\text{split}}(c - c')} \right) \quad (31)$$

The ratio $\frac{p(S_{\text{split}})}{p(S)} \approx e^{-\lambda_{\text{SH}}}$ if we choose to split the SH codebook, and $e^{-\lambda_{\text{SR}}}$ if we choose to split the SR codebook. We thus have the acceptance probability given by:

$$A(S \rightarrow S_{\text{split}}) = \min \left(1, e^{-\lambda_{\text{SH}}}/q_{sm}(u) \right) \quad (32)$$

A.1.3. Merge Codebook Vectors

Two codebook vectors c, c' can be merged into one codebook vector of value c . Two rows to be merged are selected with a transition distribution defined by:

$$q_{\text{merge}}(S \rightarrow S_{\text{merge}}) = \mathcal{N}(c - c' | \mu = 0, \sigma = \epsilon_{\text{merge}} I) \quad (33)$$

The acceptance probability of a merge transition is:

$$A(S \rightarrow S_{\text{merge}}) = \min \left(1, \frac{p(S_{\text{merge}})q_{\text{split}}(c - c')}{p(S)q_{\text{merge}}(c - c')} \right) \quad (34)$$

$\frac{p(S)}{p(S_{\text{merge}})} \approx e^{\lambda_{\text{SH}}}$ if it leads to a reduction in the number of rows, or 1 otherwise, as merging a small set of rows of codebook vectors does not affect the overall accuracy.

$$A(S \rightarrow S_{\text{merge}}) = \min \left(1, e^{\lambda_{\text{SH}}} q_{sm}(c - c') \right) \quad (35)$$

Where

$$q_{sm}(u) = \exp \left(\frac{u^2}{2} \left(\frac{1}{\epsilon_{\text{merge}}^2} - \frac{1}{\epsilon_{\text{split}}^2} \right) \right) \quad (36)$$

B. Reconstruction using an SfM Initialized Point Cloud

	DeepBlending			MipNerf360					Tanks and Temples	
	playroom	bicycle	bonsai	counter	garden	kitchen	room	stump	train	truck
3DGS	30.10	25.18	31.98	29.13	27.38	31.54	31.77	26.67	22.03	25.39
EAGLES	30.38	25.02	31.45	28.42	26.94	30.79	31.64	26.67	22.34	25.04
Reduced-GS	29.96	25.12	32.10	29.13	27.28	31.33	31.68	26.58	22.01	25.42
Scaffold-GS	30.89	25.02	32.50	29.43	27.30	31.42	32.13	26.72	22.54	25.74
SpeedySplat	30.02	25.10	31.20	28.28	26.68	29.65	30.78	26.64	21.68	25.23
Taming3DGS	30.11	24.86	32.93	29.63	27.59	32.16	32.40	26.17	22.58	26.00
ContraGS-2M	33.73	27.02	31.59	30.60	27.49	30.54	32.34	30.83	24.35	26.93

Table 4. PSNR on evaluation datasets

	DeepBlending			MipNerf360					Tanks and Temples	
	playroom	bicycle	bonsai	counter	garden	kitchen	room	stump	train	truck
3DGS	0.909	0.748	0.946	0.916	0.858	0.916	0.916	0.768	0.821	0.885
EAGLES	0.913	0.750	0.942	0.907	0.840	0.928	0.927	0.774	0.798	0.876
Reduced-GS	0.906	0.747	0.947	0.915	0.856	0.932	0.926	0.768	0.810	0.882
Scaffold-GS	0.913	0.740	0.948	0.917	0.850	0.929	0.931	0.766	0.829	0.887
SpeedySplat	0.907	0.747	0.926	0.877	0.815	0.891	0.904	0.764	0.773	0.868
Taming3DGS	0.910	0.706	0.950	0.922	0.856	0.937	0.934	0.738	0.830	0.893
ContraGS-2M	0.925	0.813	0.943	0.938	0.848	0.922	0.933	0.896	0.861	0.904

Table 5. SSIM on evaluation datasets

	DeepBlending			MipNerf360					Tanks and Temples	
	playroom	bicycle	bonsai	counter	garden	kitchen	room	stump	train	truck
3DGS	0.241	0.242	0.180	0.182	0.122	0.116	0.196	0.242	0.197	0.141
EAGLES	0.251	0.244	0.191	0.199	0.154	0.127	0.200	0.243	0.237	0.164
Reduced-GS	0.243	0.244	0.180	0.183	0.123	0.117	0.197	0.243	0.206	0.147
Scaffold-GS	0.244	0.260	0.179	0.185	0.133	0.122	0.187	0.261	0.190	0.136
SpeedySplat	0.269	0.244	0.227	0.258	0.213	0.197	0.257	0.289	0.289	0.190
Taming3DGS	0.251	0.314	0.172	0.171	0.129	0.110	0.181	0.309	0.191	0.125
ContraGS-2M	0.252	0.230	0.186	0.150	0.160	0.148	0.187	0.163	0.187	0.124

Table 6. LPIPS on evaluation datasets

	Blender								DeepBlending		MipNerf360						Tanks and Temples	
	chair	drums	figus	hotdog	lego	materials	mic	ship	playroom	bicycle	bonsai	counter	garden	kitchen	room	stump	train	truck
ContraGS-2M	158.30	127.17	236.28	-	103.08	149.54	257.87	115.33	134.57	130.04	101.38	99.03	139.62	135.20	128.97	131	128.07	96.07
3DGS	190.27	149.03	67.31	70.85	140.61	58.35	83.00	115.99	817.16	2,089.36	482.08	467.02	1,858.58	690.12	553.89	1,772.67	480.17	901.40
EAGLES	10.78	8.44	4.80	6.38	12.35	4.80	5.17	7.36	63.14	159.47	50.91	44.77	116.03	82.74	52.33	156.55	33.40	57.96
Reduced-GS	121.14	96.92	65.94	46.87	85.20	40.21	49.72	68.60	572.14	1,432.41	321.76	295.36	1,406.55	443.20	371.62	1,099.43	269.20	636.50
Scaffold-GS	31.66	31.66	31.66	31.66	31.66	31.66	31.66	31.96	95.11	304.83	135.45	91.52	246.28	107.76	89.25	252.44	114.89	192.21
SpeedySplat	72.30	57.09	43.51	32.94	61.88	32.71	32.45	50.27	393.28	895.20	314.86	264.14	1,043.39	406.80	286.05	803.08	188.92	494.39
Taming3DGS	-	-	-	-	-	-	-	-	325.63	477.60	-	631.04	1,221.08	797.98	756.10	282.02	743.60	1,189.74

Table 7. Peak memory during training

C. Random Parameter Initialization

	Tanks and Temples			MipNerf360						DeepBlending				Blender				
	train	truck	bicycle	bonsai	counter	garden	kitchen	room	stump	playroom	chair	drums	figus	hotdog	lego	materials	mic	
3DGS	19.49	18.41	17.69	16.46	23.46	21.71	24.61	27.69	20.74	14.41	31.93	24.91	29.05	36.48	32.37	29.69	34.58	
EAGLES	18.91	18.43	19.30	17.79	23.25	24.82	25.52	25.27	20.08	20.82	34.42	25.68	33.67	37.05	34.92	28.95	35.12	
Reduced-GS	18.74	18.02		15.59	23.85	24.15	25.82	25.11	19.67	12.95	35.59	26.28	35.48	38.07	36.06	30.50	36.71	
Scaffold-GS	19.69	18.32	20.58	17.77	21.06	18.45	23.08	23.35	18.73	13.99	34.85	26.17	35.04	37.81	35.42	30.60	36.69	
SpeedySplat	19.24	18.15	15.90	19.54	23.84	0.00	0.00	24.40	0.00	13.39	33.95	25.96	35.18	36.13	32.12	29.33	35.86	
Taming3DGS	19.78	18.46	19.64	20.08	-	-	26.73	-	20.86	-	-	-	-	-	-	-	-	
ContraGS-2M	24.35	26.93	27.02	31.59	30.60	27.49	30.54	32.34	30.83	33.73	38.48	29.05	38.79	36.48	39.34	36.20	41.56	

Table 8. PSNR measured on evaluation dataset

	Tanks and Temples			MipNerf360						DeepBlending				Blender				
	train	truck	bicycle	bonsai	counter	garden	kitchen	room	stump	playroom	chair	drums	figus	hotdog	lego	materials	mic	
3DGS	0.737	0.722	0.487	0.658	0.827	0.710	0.878	0.870	0.606	0.682	0.983	0.941	0.953	0.984	0.975	0.950	0.987	
EAGLES	0.726	0.719	0.562	0.690	0.835	0.784	0.890	0.846	0.600	0.808	0.984	0.950	0.982	0.983	0.980	0.949	0.989	
Reduced-GS	0.717	0.712	-	0.620	0.840	0.762	0.891	0.838	0.567	0.646	0.988	0.955	0.987	0.985	0.983	0.960	0.992	
Scaffold-GS	0.727	0.696	0.467	0.697	0.780	0.455	0.830	0.803	0.396	0.669	0.985	0.948	0.985	0.984	0.980	0.960	0.992	
SpeedySplat	0.706	0.701	0.422	0.713	0.816	-	-	0.817	-	0.657	0.979	0.949	0.985	0.975	0.958	0.947	0.990	
Taming3DGS	0.743	0.722	0.525	0.735	-	-	0.895	0.000	0.588	-	-	-	-	-	-	-	-	
ContraGS-2M	0.861	0.904	0.813	0.943	0.938	0.848	0.922	0.933	0.896	0.925	0.993	0.977	0.994	0.984	0.992	0.989	0.997	

Table 9. SSIM measured on evaluation dataset

	Tanks and Temples				MipNerf360					DeepBlending				Blender			
	train	truck	bicycle	bonsai	counter	garden	kitchen	room	stump	playroom	chair	drums	figus	hotdog	lego	materials	mic
3DGS	0.286	0.291	0.481	0.469	0.289	0.251	0.182	0.279	0.398	0.549	0.023	0.059	0.043	0.030	0.031	0.064	0.026
EAGLES	0.306	0.305	0.422	0.443	0.273	0.203	0.174	0.312	0.406	0.387	0.015	0.045	0.018	0.025	0.020	0.053	0.011
Reduced-GS	0.307	0.308	-	0.498	0.277	0.219	0.168	0.320	0.441	0.308	0.010	0.036	0.012	0.020	0.016	0.037	0.006
Scaffold-GS	0.291	0.317	0.505	0.456	0.353	0.508	0.262	0.368	0.571	0.573	0.014	0.047	0.014	0.023	0.019	0.041	0.008
SpeedySplat	0.349	0.359	0.567	0.427	0.327	-	-	0.352	0.000	0.581	0.023	0.048	0.014	0.044	0.060	0.061	0.011
Taming3DGS	0.282	0.292	0.454	0.404	-	-	0.161	-	0.406	-	-	-	-	-	-	-	-
ContraGS-2M	0.187	0.124	0.230	0.186	0.150	0.160	0.148	0.187	0.163	0.252	0.007	0.026	0.007	0.030	0.009	0.019	0.003

Table 10. LPIPS measured on evaluation dataset

D. Training and Rendering Speeds

	T and T				MipNerf360					DeepBlending
	train	truck	bicycle	bonsai	counter	garden	kitchen	room	stump	playroom
Taming3DGS	263.40	240.66	224.62	211.51	170.02	178.84	163.10	174.79	374.40	468.09
Ours 5M	129.00	96.00	89.00	58.00	46.00	118.00	101.00	107.00	88.00	141.00
Ours	206.00	209.00	159.00	217.00	219.00	249.19	210.00	242.00	220.00	319.00
MCMC 5M	75.50	85.90	72.00	68.50	56.10	91.70	59.49	71.24	41.00	114.00
MCMC 2M	94.00	173.32	77.00	75.69	62.78	185.00	70.16	143.58	142.79	251.8

Table 11. Frames per second (FPS) measured on differnt datasets

	DeepBlending	MipNerf360							T and T	
	playroom	bicycle	bonsai	counter	garden	kitchen	room	stump	train	truck
MCMC 2M	31.66	24.00	24.00	20.00	27.00	22.87	23.70	24.00	29.19	31.49
MCMC 5M	13.10	11.99	11.99	10.09	13.08	10.81	11.28	12.76	12.25	13.65
Ours	46.33	31.63	27.07	32.82	36.33	29.48	34.80	32.00	38.50	43.00
Ours 5M	21.65	15.09	13.55	11.59	17.80	13.14	17.45	17.33	19.87	18.48
Taming3DGS	93.12	71.35	50.09	48.59	40.02	40.70	49.09	102.78	67.08	47.11

Table 12. Training Iterations per second

D.1. Comparison of Training Speeds with Taming-GS at Different Gaussian Counts

Table 13 compares training speeds with TamingGS.

Model-numGS	PSNR	Training time	Memory
ContraGS-2M	30.06	14 mins	130 MB
ContraGS-530K	29.31	6.5 mins	59 MB
TamingGS	29.39	8 mins	477 MB

Table 13. Performance comparison of TamingGS and ContraGS for the same number of Gaussians

E. Qualitative Results

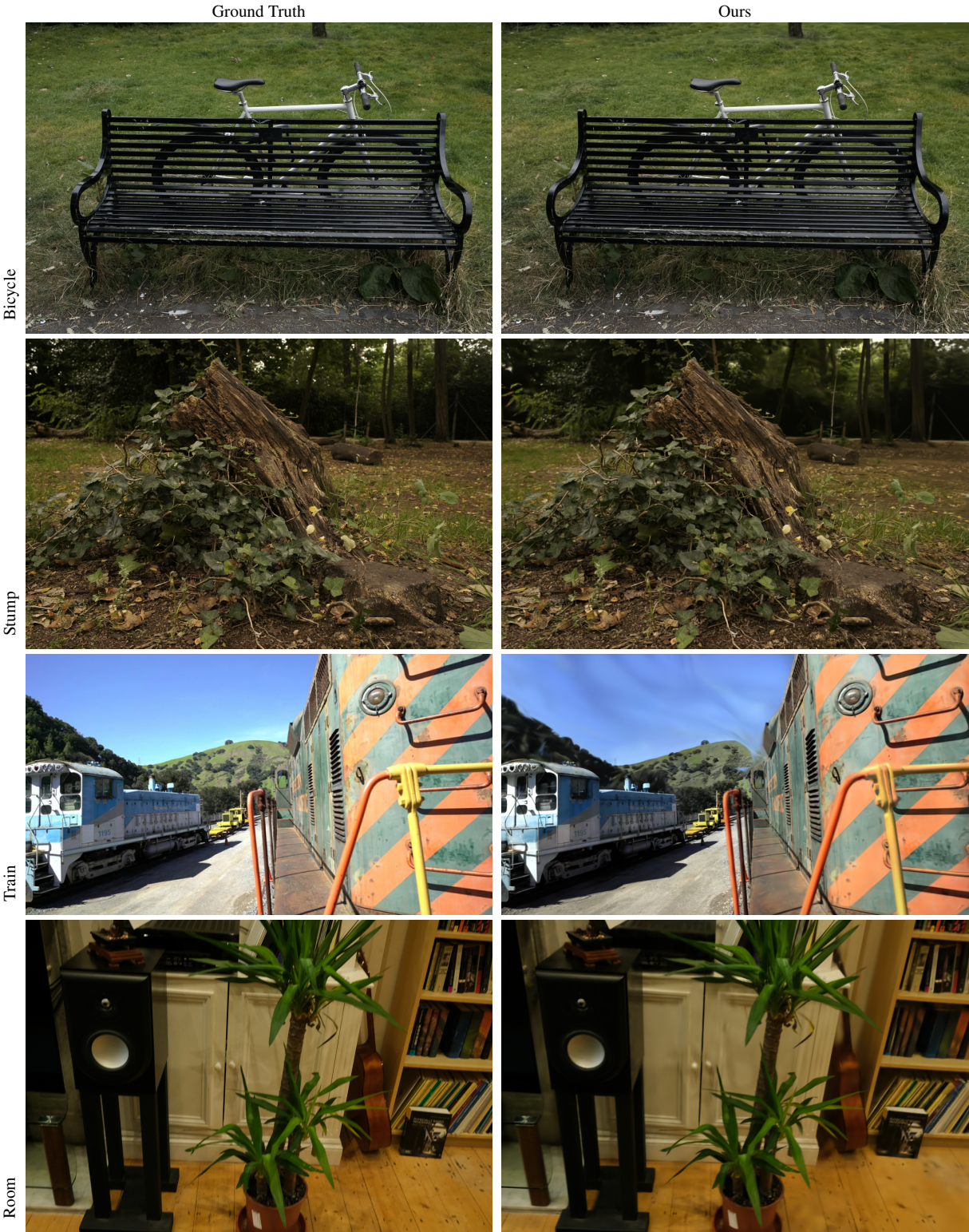


Figure 8. Qualitative results of ContraGS compared to ground truth reconstruction